Simultaneous and Proportional Control of Wrist and Hand Movements Based on a Neural-Driven Musculoskeletal Model

Jianmin Li, *Member, IEEE*, Shizhuo Yue, and Lizhi Pan, *Member, IEEE*

***Abstract*— Human-machine interfaces (HMIs) based on electromyography (EMG) signals have been developed for simultaneous and proportional control (SPC) of multiple degrees of freedom (DoFs). The EMG-driven musculoskeletal model (MM) has been used in HMIs to predict human movements in prosthetic and robotic control. However, the neural information extracted from surface EMG signals may be distorted due to their limitations. With the development of high density (HD) EMG decomposition, accurate neural drive signals can be extracted from surface EMG signals. In this study, a neural-driven MM was proposed to predict metacarpophalangeal (MCP) joint flexion/extension and wrist joint flexion/extension. Ten non-disabled subjects (male) were recruited and tested. Four 64-channel electrode grids were attached to four forearm muscles of each subject to record the HD EMG signals. The joint angles were recorded synchronously. The acquired HD EMG signals were decomposed to extract the motor unit (MU) discharge for estimating the neural drive, which was then used as the input to the MM to calculate the muscle activation and predict the joint movements. The Pearson's correlation coefficient (r) and the normalized root mean square error (NRMSE) between the predicted joint angles and the measured joint angles were calculated to quantify the estimation performance. Compared to the EMG-driven MM, the neural-driven MM attained higher r values and lower NRMSE values. Although the results were limited to an offline application and to a limited number of DoFs, they indicated that the neural-driven MM outperforms the EMG-driven MM in prediction accuracy and robustness. The proposed neural-driven MM for HMI can obtain more accurate neural commands and may have great potential for medical rehabilitation and robot control.**

***Index Terms*— Electromyography, neural drive, human–machine interface, musculoskeletal model, motor unit.**

Manuscript received 10 May 2023; revised 3 September 2023 and 27 September 2023; accepted 1 October 2023. Date of publication 10 October 2023; date of current version 18 October 2023. This work was supported in part by the National Natural Science Foundation of China under Grant 52005364 and Grant 52122501 and in part by the Key Laboratory of Mechanism Theory and Equipment Design of Ministry of Education (Tianjin University). *(Corresponding author: Lizhi Pan.)*

This work involved human subjects or animals in its research. Approval of all ethical and experimental procedures and protocols was granted by the Ethics Committee of Tianjin University under Approval No. TJUE-2021-114, and performed in line with the Declaration of Helsinki.

The authors are with the Key Laboratory of Mechanism Theory and Equipment Design of Ministry of Education, School of Mechanical Engineering, Tianjin University, Tianjin 300350, China (e-mail: mjli@tju.edu.cn; szyue@tju.edu.cn; melzpan@tju.edu.cn).

Digital Object Identifier 10.1109/TNSRE.2023.3323347

I. Introduction

ELECTROMYOGRAPHY (EMG) signals contain rich physiological information and have been widely used as inputs of human-machine interfaces (HMIs) to decode movement intentions, mainly involving prosthesis control [1], medical rehabilitation equipment control [2], and remote robot control [3]. In order to achieve the control of multiple joints, the HMIs based on EMG signals are developing towards simultaneous and proportional control (SPC) of multiple degrees of freedom (DoFs). Model-free data-driven approaches have been developed to map EMG signals to joint kinematics, such as non-negative matrix factorization (NMF) [4], linear regression (LR) [5], support vector regression (SVR) [6], artificial neural network (ANN) [7], and deep learning (DL) approaches [8], [9], [10], [11], [12], [13], [14], [15]. Ma et al. used a bi-directional long short-term memory (Bi-LSTM) network to simultaneously and proportionally estimate the movements of the non-dominant arm based on the sEMG signals of the muscles on the corresponding dominant arm [13]. Liu et al. proposed a NeuroPose system that combines recurrent neural network (RNN), encoder-decoder network, and machine learning on ResNets to extract 3D finger movements from the EMG data [14]. Lin et al. proposed a method based on the transformer bidirectional encoder representation (BERT) structure, using surface EMG signals to predict hand movements [15]. Although data-driven approaches have good performance for movement prediction, they lack the ability for learning transfer and require more time to calibrate the controllers [16], [17]. To achieve more intuitive and natural myoelectric control, it is necessary to take into account the physiological mechanisms of the human body and the complicated conversion process from the neural commands to the joint movements [18], [19].

The approaches based on the musculoskeletal model (MM) do consider the above issues. The MM is modeled through muscle activation, contraction dynamics, kinematics, and joint mechanics, which can convert neural commands into mechanical outputs [20], [21]. The HMIs based on EMG-driven MM have been developed to predict joint torques and joint angles during dynamic joint movements [16], [17], [20], [22], [23], [24]. Crouch et al. proposed a two-DoF lumped-parameter MM by combining four forearm mus-

cles into two pairs of antagonistic muscles to predict wrist joint flexion/extension and metacarpophalangeal (MCP) joint flexion/extension [22]. Pan et al. compared the performance of MM-based approach with that of LR and ANN algorithms in predicting joint angles from surface EMG signals [16]. The results demonstrated that the MM-based approach outperformed the LR and ANN algorithms, and the predicted joint angles by the former were closer to the measured joint angles. Model-based approaches have greater physical significance than data-driven approaches because they consider the physiological mechanisms of the human body.

In the EMG-driven MM, muscle activation is estimated from the magnitude of the EMG signals (the envelope of EMG). Therefore, the quality of surface EMG signals affected the estimated muscle activation level, and then affected the reliability of prediction for force and joint movements. If the activation of the target muscle acquired by the EMG electrode was affected by the activation of adjacent muscles, the muscle activation level and joint angles would be incorrectly estimated. As demonstrated in the previous studies, the prediction accuracy of MCP joint angles was lower during multi-joint movements than during single-joint movements, which may be attributed to the crosstalk of EMG signals during MCP movement when the wrist moved simultaneously [22]. Inspired by muscle synergy, Zhao et al. proposed a new muscle activation extraction method and a synergy-based MM for simultaneous estimation of hand and wrist movements [17]. The results demonstrated that the performance of the synergy-based MM was better than that of the EMG-driven MM, and the synergy-based MM can also extract more accurate muscle activation despite crosstalk between the wrist and MCP joints during simultaneous movements. The synergy-based MM provided a perspective for combining the MM to predict continuous movements.

Surface EMG signals are a series of transitions of neural commands from the brain or spinal cord to muscles, which are acquired from the skin surface above the muscles. In fact, the EMG signals are the superposition of the motor unit action potential (MUAP) trains of the recruited MUs in space and time. The phase and amplitude cancellation between MUAPs during superposition can affect the EMG amplitude [25]. The volume conduction from muscle to skin surface affects the amplitude or shape of the MUAPs. These may lead to the distortion of neural information in the acquired EMG signals. The development of high density (HD) EMG decomposition allows the extraction of accurate neural commands from surface EMG signals. The discharge of MUs is obtained by decomposing the acquired HD EMG signals. The discharge of recruited MUs is represented as the binary motor unit spike trains (MUSTs), and can overcome the influence of MUAP change during signal acquisition [26]. The number of discharges by the motor neurons in the muscle reflects the neural drive from the brain or spinal cord to the muscle [27]. The neural drive signal is calculated from the normalized frequency of the composite discharge of the motor unit pool obtained by the decomposition [28]. The neural drive signals can directly reflect the neural commands from the brain to the muscle and can be used to estimate the level of muscle activation. The HD EMG decomposition technology helps to better understand the neural regulation mechanism of movement and has been widely used in the field of HMIs [26], [29], [30]. The robustness of HD EMG decomposition in dynamic movement has been demonstrated [29], [30]. Previous studies have demonstrated that it is more accurate to predict force or joint movement with neural drive signals was more accurate than with EMG signals [28], [31]. However, it requires further study to check whether the neural drive signals can improve the performance of MM in predicting joint movements.

In this study, a neural-driven MM was proposed to estimate the continuous movements of the wrist and MCP joint. The purpose of this study was to develop an HMI that conformed to human physiology at the neural level to achieve more intuitive and natural myoelectric control. Neural drive signals were decomposed from HD EMG signals to replace the envelopes of EMG to estimate muscle activation levels. Ten non-disabled subjects were recruited and tested. The HD EMG signals and joint angles of each subject were recorded simultaneously. The performance of the neural-driven MM in predicting wrist and MCP joint movements was evaluated by calculating the Pearson's correlation coefficient (r) and the normalized root mean square error (NRMSE) between the measured and estimated joint angles. The performance of the neural-driven MM was compared with that of the EMG-driven MM. A preliminary study involving one subject has been reported in a conference [32].

II. Methods

A. Subjects

Ten non-disabled subjects (males, aged 22-26 years, all right hand dominant) participated in the study. All subjects had no neuromuscular or joint diseases. Before the experiment, subjects were informed about the procedure and signed informed consent forms. The experimental protocol followed the Declaration of Helsinki and was approved by the Ethics Committee of Tianjin University (Approval #: TJUE-2021-114).

B. Experiment Protocol

The subjects sat naturally on the straight back chair and put their forearms on the armrest in a neutral position (see Fig. 1). The MCP joints of the four fingers were completely relaxed and naturally bent to the palm (see Fig. 2). During the experiment, the subjects performed the following five tasks: (1) wrist flexion/extension only, rhythm; (2) wrist flexion/extension only, random; (3) MCP flexion/extension only, rhythm; (4) MCP flexion/extension only, random; (5) wrist and MCP flexion/extension simultaneously, random.

During the rhythm trials, the subjects performed cyclical movements at a fixed frequency (1/4 Hz), from the initial position to the maximum angle in either direction of each DoF. During the random trials, the subjects performed random movements with variable speeds and joint angles.

During the experiment, the subjects performed 10 trials for each task. Each trial lasted for 30 seconds. In order to avoid muscle fatigue, the subjects rested for 1 minute between

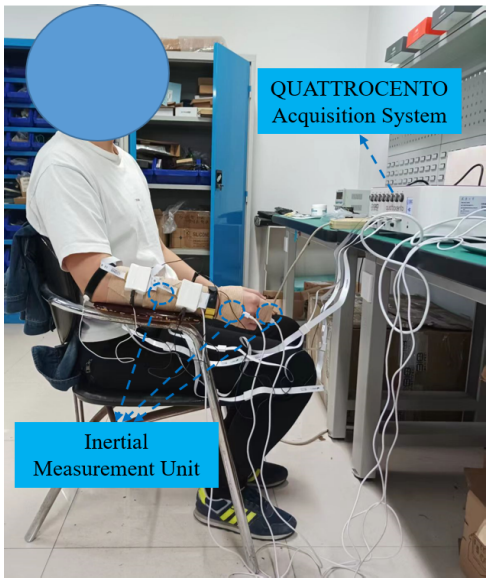

Fig. 1. Experiment setup and the initial neutral posture.

two consecutive trials. Each subject performed a total of 50 trials (5 tasks × 10 trials).

C. Data Acquisition

The surface EMG signals of forearm muscles were acquired with the HD electrode grids (GR10MM0808, OT Bioelettronica, Italy). Before the electrode grids were placed, the gel was applied to each electrode to increase conductivity, and the corresponding skin was cleaned with an alcohol pad to reduce the impedance between the skin and the electrodes. The subjects were required to flex or extend the wrist or MCP joint, and the bellies of muscles were determined by palpating the corresponding muscles, over which the electrode grids were placed. Four 8 × 8 flexible HD electrode grids (with 10 mm distance between adjacent electrodes in both directions) were placed on the following four muscles of the forearm: (1) extensor digitorum; (2) extensor carpi radialis; (3) flexor digitorum; (4) flexor carpi radialis (see Fig. 2). The electrode grids were fixed with elastic bandages to prevent electrode shift during the experiment. The ground strap was placed on the wrist while the reference strap was placed on the elbow. The QUATTROCENTO (OT Bioelettronica, Italy) acquisition system amplified and filtered the monopolar EMG signals (with a fixed gain of 150 V/V, a band-pass filter of 10-500 Hz, and a sampling rate of 5120 Hz).

The angles of the wrist and MCP joint were acquired simultaneously using the inertial measurement unit (IMU, Dongguan Wheeltec Technology Co., China). In this study, three IMUs were placed over the forearm, the back of the palm, and the back of the fingers near the MCP joint (see Fig. 1). The IMUs were all fixed with elastic bandages to prevent shift or falling during the experiment. The joint angles of these two DoFs were recorded at a sampling rate of 200 Hz.

D. Data Analysis

All the acquired EMG signals were preprocessed with a 4-order Butterworth band-pass filter (10-500 Hz) and a notch

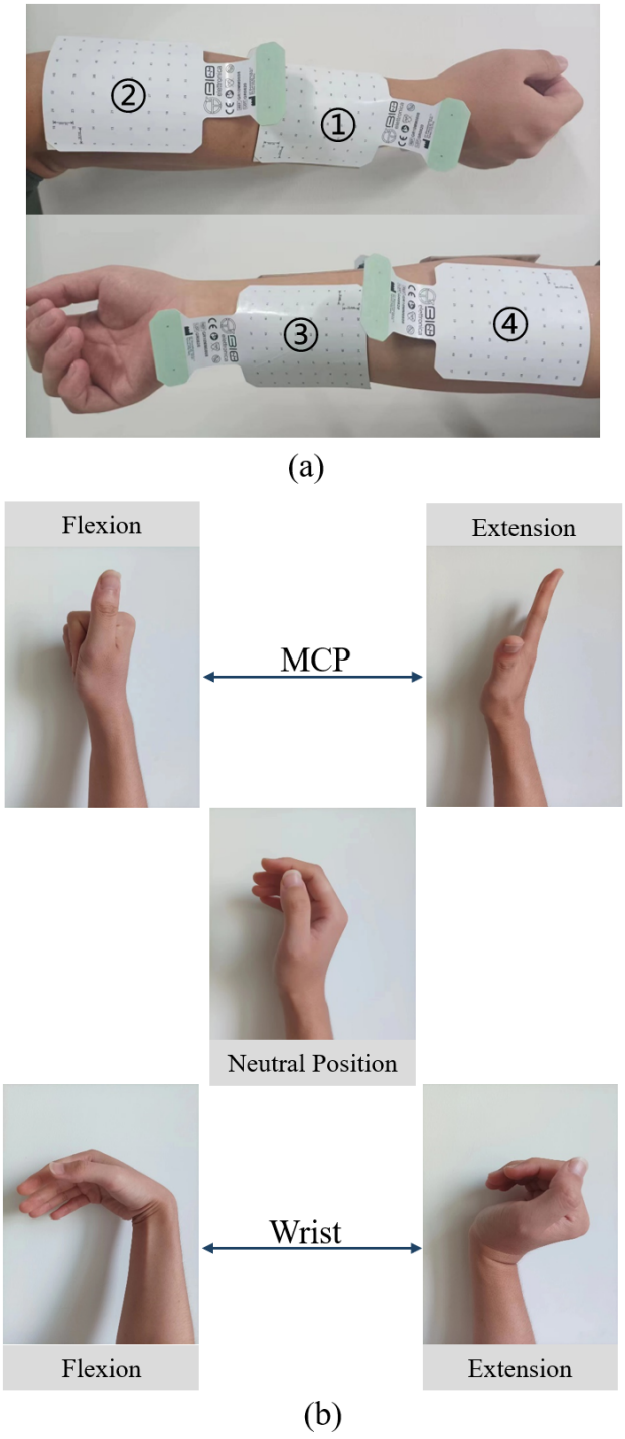

Fig. 2. (a) The placement of four 8 × 8 high-density electrode grids. (b) The neutral position of the wrist and MCP joint, and the maximum joint angle of MCP and wrist extension/flexion.

filter (50 Hz and its multiples). The 256-channel EMG signals acquired from each trial were checked by calculating the root mean square (RMS) and visual inspection. The abnormal data channels that contain excessive noise caused by poor contact or electromagnetic interference were removed, as well as the channels with extremely low RMS values at the edge of the electrode grid. For each electrode grid, less than 5 channels

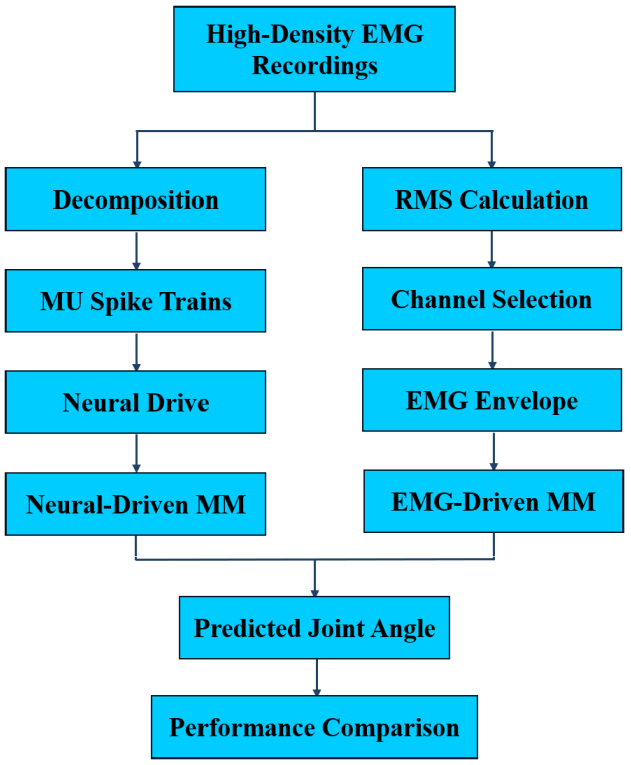

Fig. 3. Block diagram of the data analysis.

were removed. The EMG recordings of the remaining channels were used for analysis. The block diagram of the data analysis procedure was illustrated in Fig. 3.

The EMG signals were the convolution of MUSTs and their respective MUAPs. EMG signal decomposition could be regarded as a classic blind source separation problem, which could be achieved by independent component analysis (ICA) [33]. The fast ICA (FastICA) algorithm has been demonstrated to be feasible in decomposing the HD EMG signals acquired during dynamic contraction [30].

The following steps briefly describe the process of extracting MU from 64-channel EMG signals [34], [35], [36]. (1) The EMG signals were extended and whitened. Altogether 200 sources were assumed to provide the algorithm more opportunities to converge to the activated MUs. The EMG signals were extended by adding the delayed replicas (extension factor R = 4) to ensure that there were more channels than the unknown sources [36], [37]. Then the extended EMG signals were whitened by eigenvalue decomposition. (2) The source signals and separation matrix were obtained with FastICA algorithm to decompose the extended and whitened EMG signals. (3) The K-means clustering algorithm [38] (cluster number = 2) was used to extract the MUSTs, so as to distinguish the MU discharge of the source signals and the baseline noise. (4) The MUSTs with silhouette measure (SIL) less than 0.8 were removed (SIL is an effective clustering index to evaluate the quality of clustering [30], [39]). Because the delayed replicas were added during extension of the EMG signals, the source signals obtained by convergence may be the same MU or its delayed replicas. If the synchronization of two MUSTs was larger than 50% in the ±1 ms window, the two MUs were considered to be the same.

For any two repeated MUs, only the MUST with a higher SIL value was retained. The MUs were estimated as:

$$\hat{S}_j(t) = W_j{}^T \hat{X}(t) \tag{1}$$

where $\hat{X}$ represents the extended and whitened EMG signals, t represents the time of sampling points, $\hat{S}_j$ represents the jth source signal, and W_j represents the separation vector and provides the source signal $\hat{S}_j$ corresponding to information of the jth MU.

The EMG signals of the first rhythm trial of the wrist and MCP joint were used for MU decomposition. The separation matrices of the four muscles were retained. The EMG signals from other trials were extended and whitened, which were then multiplied with the retained separation matrices to directly estimate the source signals [40], [41].

The retained MU spike trains were pooled into composite spike trains, whose normalized discharge frequency was calculated to estimate the neural drive of each muscle. A sliding window of 200 ms window length and 50 ms step length was applied to calculate the average discharge frequency of the composite spike trains [26].

To predict the joint movements, a neural-driven MM was developed based on a previous lumped-parameter EMG-driven MM [22]. The MM included two DoFs, wrist flexion/extension and MCP flexion/extension, which allowed wrist and MCP joint to move independently in both directions. To simplify the modeling, only two pairs of antagonistic muscles were included in the MM. The extensor digitorum and flexor digitorum cross the wrist and MCP joints. The extensor carpi radialis and flexor carpi radialis only passed through the wrist joint, with no moment arm at the MCP joint. The following six parameters of each muscle were optimized with the optimization function GlobalSearch in MATLAB: optimal muscle length, maximum isometric force, moment arm of the wrist joint, moment arm of the MCP joint, muscle length at the neutral position, and parallel elastic element stiffness. In the optimization process, all parameters were limited to the approximate range of physiological values to minimize the root mean square error between the predicted and measured joint angles.

Since the electrode grids were placed over the bellies of muscles, the amplitude of the EMG signals acquired by the channels located at the edge of the electrode grids or the edge of the muscles was low. Moreover, since there were still crosstalks in the EMG signals acquired by HD electrode grids, directly averaging 64-channel EMG signals could not represent muscle activation well. The channel selection method was used to find the best activation area of the muscle, which helped to avoid the influence of low amplitude channels and determine the optimal muscle activation area to reduce signal crosstalk during simultaneous movements of two DoFs. The RMS value of 64-channel signals was calculated and normalized.

The 2 × 2 channels were selected as the optimal activation area of each muscle (see Fig. 4). The EMG signals of these channels were averaged and then full-wave rectified. The rectified signals were low-pass filtered by a 5-Hz 4-order Butterworth filter and then filtered by a moving root mean square filter (window length: 1024 sampling points,

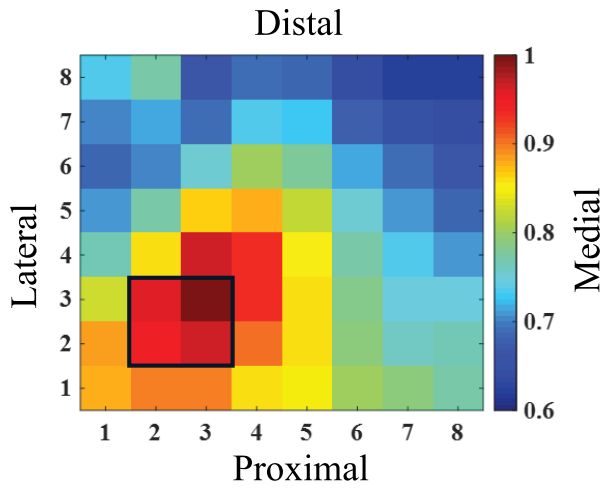

Fig. 4. Two-dimensional heat map (the normalized RMS value) of the flexor digitorum during MCP joint movement. The black box shows the optimal activation position for the muscle. The four directions of proximal, distal, lateral and medial are indicated respectively.

step length: 256 sampling points) to obtain the EMG envelope. Finally, the EMG envelope was normalized by the maximum EMG acquired during maximum voluntary contraction.

E. Evaluation Metrics

The performance of the neural-driven MM in predicting wrist and MCP joint angles was evaluated and compared with that of the EMG-driven MM. The r and the NRMSE between the predicted joint angles and the measured joint angles were calculated as the evaluation metrics of the model.

$$r = \frac{\sum_{i=1}^{n} (x_i - \bar{x}) \cdot (y_i - \bar{y})}{\sqrt{\sum_{i=1}^{n} (x_i - \bar{x})^2 \cdot (y_i - \bar{y})^2}} \tag{2}$$

$$NRMSE = \frac{\sqrt{\frac{1}{n} \sum_{i=1}^{n} (x_i - y_i)^2}}{x_{max} - x_{min}} \tag{3}$$

where x_i is the ith measured joint angle, $\bar{x}$ is the mean value of the measured joint angles, y_i is the ith predicted joint angle, $\bar{y}$ is the mean value of the predicted joint angles, n is the length of the data sampling point, x_{max} is the maximum value of the measured joint angles, and x_{min} is the minimum value of the measured joint angles.

F. Statistical Analysis

A three-way repeated measures analysis of variance (ANOVA) was performed on r values and NRMSE values. The three independent variables were algorithm (neural-driven MM and EMG-driven MM), DoF (wrist extension/flexion, MCP extension/flexion), and movement type (single-DoF movement, simultaneous movement). Johnson transformation was performed on data that did not conform to the normal distribution to ensure that all data conform to the normal distribution before variance analysis. A statistical model was established to study whether there was a significant interaction between the three independent variables. If a significant interaction between variables was found, a simple impact analysis of the level of interaction factors was required. If no interaction was found, a reduced ANOVA without interaction effect was performed on r values and NRMSE values by taking algorithm, DoF, and movement type as the independent variable respectively. The significance level for all tests was set to $p = 0.05$.

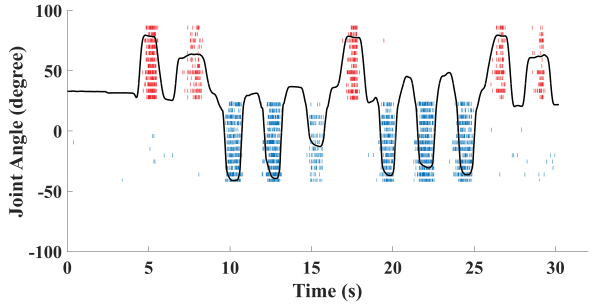

Fig. 5. The motor units of extensor and flexor digitorum retained during a random trial of MCP flexion/extension only. Each bar represents a discharge. The MCP joint angle of this random trial was recorded synchronously, represented by a black trace.

III. Results

Fig. 5 shows an example of a series of MU discharge trains that were obtained by decomposing the representative HD EMG with the FastICA algorithm, and the corresponding joint angles were recorded synchronously. It can be intuitively observed that the size of the joint angle affects the continuous discharge of MUs.

Fig. 6(a) and Fig. 6(b) show the r values of the neural-driven MM and EMG-driven MM during single-DoF movements and simultaneous movements of all subjects, respectively. For the neural-driven MM, the mean r values of wrist and MCP joints during single-DOF movements were 0.93 and 0.91, respectively. The mean r values of wrist and MCP joints during simultaneous movements were 0.91 and 0.86, respectively. For the EMG-driven MM, the mean r values of the wrist and MCP joints during single-DOF movements were 0.90 and 0.87, respectively. During the simultaneous movements of two DoFs, the mean r values of wrist and MCP joints were 0.88 and 0.76, respectively. The three-way ANOVA showed no significant three-way or two-way interaction among the variables of algorithm, DoF, and movement type. Then the reduced ANOVA showed that algorithm, DoF, and movement type had a significant effect on r (DoF: $0.001 < p \leq 0.01$, movement type: $0.001 < p \leq 0.01$). Fig. 6 shows the significant difference of algorithm.

Fig. 7(a) and Fig. 7(b) show the NRMSE values of the neural-driven MM and EMG-driven MM during single-DoF movements and simultaneous movements of all subjects, respectively. For the neural-driven MM, the mean NRMSE values of wrist and MCP joints during single-DOF movements were 0.12 and 0.14, respectively. The mean NRMSE values of wrist and MCP joints during simultaneous movements were 0.13 and 0.20, respectively. For the EMG-driven MM, the mean NRMSE values of the wrist and MCP joints during single-DOF movements were 0.16 and 0.22, respectively. During the simultaneous movements of two DoFs, the mean NRMSE values of wrist and MCP joints were

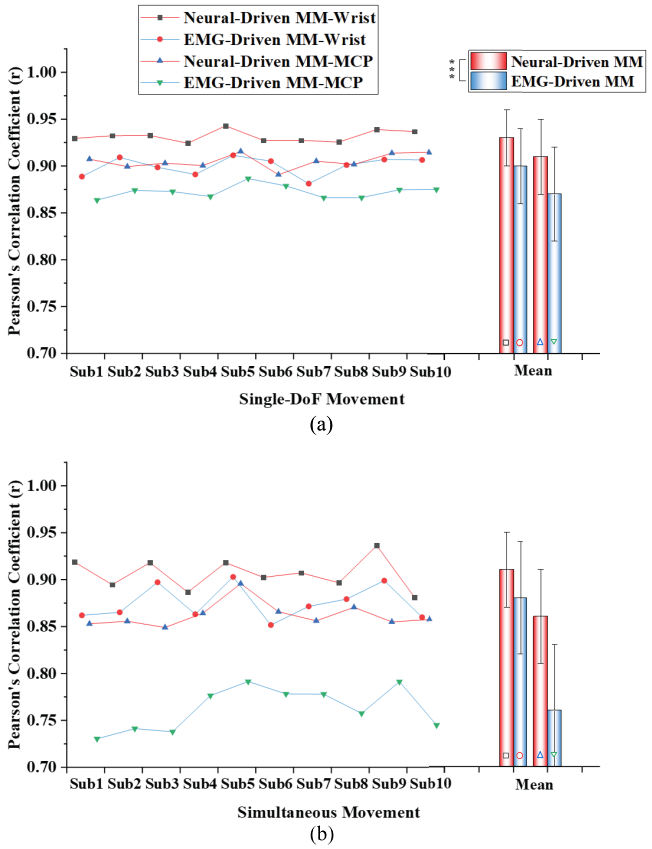

Fig. 6. Pearson's correlation coefficient (r) of neural-driven MM and EMG-driven MM during different joint movements of all subjects. The rightmost four bars are the mean values across all subjects, the error bars represent standard deviations across all subjects. Symbols $*$, $**$, and $***$ indicate significant differences with a level of ($0.01<p<0.05$), ($0.001<p \leq 0.01$), and ($p \leq 0.001$), respectively.

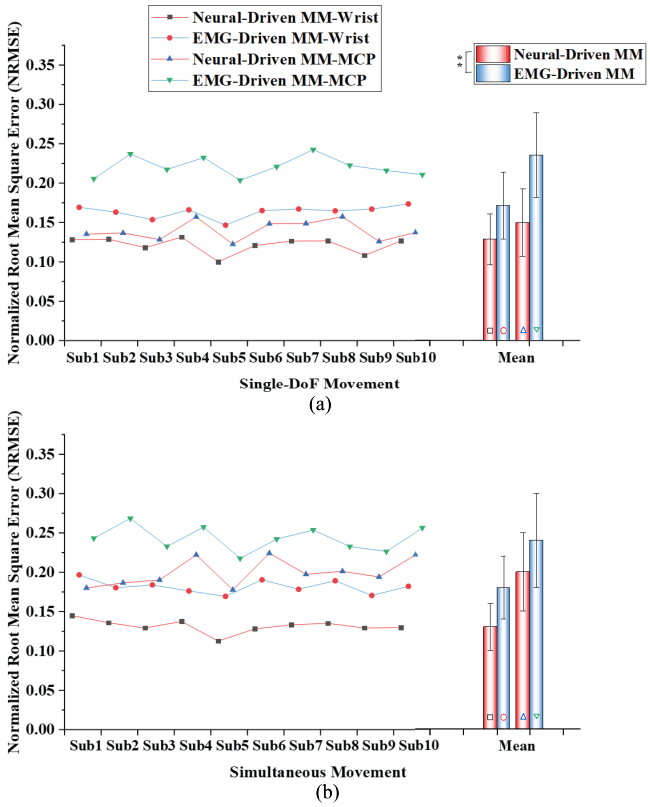

Fig. 7. NRMSE of neural-driven MM and EMG-driven MM during different joint movements of all subjects. The rightmost four bars are the mean values across all subjects, the error bars represent standard deviations across all subjects. Symbols $*$, $**$, and $***$ indicate significant differences with a level of ($0.01<p<0.05$), ($0.001<p \leq 0.01$), and ($p \leq 0.001$), respectively.

0.18 and 0.24, respectively. The three-way ANOVA showed no significant three-way or two-way interaction among the variables of algorithm, DoF, and movement type. Then the reduced ANOVA showed that algorithm, DoF, and movement type had a significant effect on NRMSE (DoF: $0.001<p \leq 0.01$, movement type: $0.01<p<0.05$). Fig. 7 shows the significant difference of algorithm.

Fig. 8 shows the predicted and measured joint angles of the wrist and MCP joint during the rhythm trial and the two-DoF simultaneous trial. Fig. 8(a) shows the extension/flexion of the wrist joint during the rhythm trial. For the neural-driven MM, the r value of wrist joint was 0.940, and the NRMSE value was 0.100. For the EMG-driven MM, the r value of wrist joint was 0.889, and the NRMSE value was 0.155. Fig. 8(b) shows the extension/flexion of the MCP joint during the rhythm trial. For the neural-driven MM, the r value of the MCP joint was 0.919, and the NRMSE value was 0.128. For the EMG-driven MM, the r value of the MCP joint was 0.878, and the NRMSE value was 0.183. Fig. 8(c) shows the predicted angles of the two joints in the two-DoF simultaneous trial. For the neural-driven MM, the r values of wrist and MCP joints were 0.923 and 0.907, respectively, and the NRMSE values of wrist and MCP joints were 0.108 and 0.140, respectively. For the EMG-driven MM, the r values of wrist and MCP joints were 0.892 and 0.723, respectively, and the NRMSE values of wrist and MCP joints were 0.129 and 0.207, respectively. Although both models can accurately predict joint angles, the joint angles predicted by the neural-driven MM are closer to measured values than those by the EMG-driven MM.

IV. Discussion

In this study, a neural-driven MM was proposed to predict MCP flexion/extension and wrist flexion/extension to improve the estimation performance of model-based approaches. HD EMG signals were acquired from four electrode grids. The 64-channel EMG signals were decomposed into individual MUSTs, and the recruited MU discharge frequency was used to calculate the neural drive signal and estimate joint kinematics. The proposed neural-driven MM used the FastICA algorithm to decompose the surface EMG signals for obtaining accurate neural drive signals and then took these signals as the input to predict joint movements. The separation parameters obtained by MU decomposition were used for random dynamic contraction and two-DoF movements. The performance of neural-driven MM for joint movements estimation was compared with that of the traditional EMG-driven MM. The r values and NRMSE values between the predicted joint angles and the measured joint angles were calculated to quantify the estimation performance of two models. The results

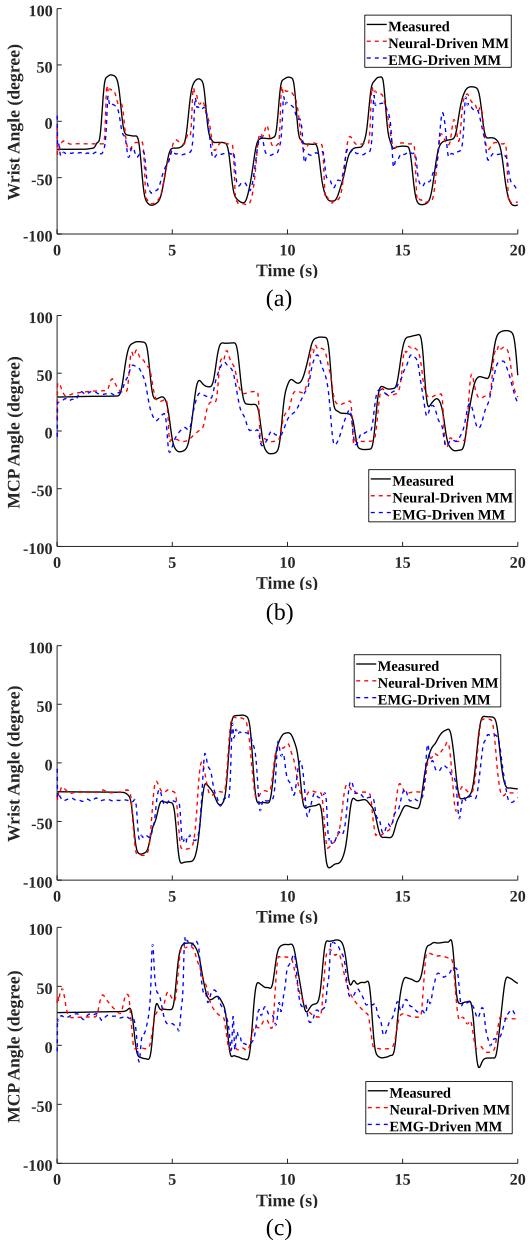

Fig. 8. Predicted and measured joint angles during (a) wrist flexion/extension only, rhythm; (b) MCP flexion/extension only, rhythm; (c) wrist and MCP flexion/extension simultaneously.

indicated that the prediction accuracy of the neural-driven MM outperforms that of the EMG-driven MM in offline analysis.

As indicated in Fig. 6 and Fig. 7, the neural-driven MM achieved higher r values and lower NRMSE values than those of the EMG-driven MM. It was demonstrated that the neural-driven MM had the superiority of joint movement prediction accuracy in offline analysis. Statistical analysis of r values and NRMSE values showed that there were significant differences between the neural-driven MM and the EMG-driven MM. The mean r values of the neural-driven MM were higher than that of the EMG-driven MM in all tasks. In particular, the predicted r value of the MCP joint movements was 0.86 during the two-DoF simultaneous movements, which was increased by 0.10. The r values of the wrist and MCP joint movements predicted by the neural-driven MM were all above 0.85, which indicated that the proposed approach could attain high-level estimation accuracy during both single-DoF movements and two-DoF simultaneous movements. Although both neural-driven MM and EMG-driven MM were modeled based on MM, the neural-driven MM had better performance, indicating that the proposed approach can extract more accurate neural information. The estimation accuracy of the neural-driven MM during two-DoF simultaneous movements was consistent with that previously reported in a conference [32].

The five different tasks used in this experiment were designed based on previous studies [16], [22], involving both cyclical dynamic movements and random dynamic movements. The performance of the proposed approach was systematically tested with these tasks. The 1/4 Hz frequency was selected in the rhythm trials because the movement of MCP and wrist at this speed was considered to be more representative of daily life [22]. As demonstrated in previous studies, the FastICA algorithm can extract MU discharge in dynamic movements. Dai et al. used the FastICA algorithm to decompose the signals of extensor digitorum for predicting the joint angle of the finger extension [30]. In this study, the FastICA algorithm was used to decompose the EMG signals acquired by each muscle in the first trial of single-DoF rhythmic movements to obtain the separation matrix, which was then applied to the decomposition of subsequent trials. By doing so, the EMG decomposition is actualy divided into two steps, which brings the following benefits. (1) Using the online decomposition approach to do offline analysis can facilitate the future study on online performance. (2) The separation matrix obtained by single-joint movements can be directly used for simultaneous movements of two joints to demonstrate the robustness of the separation matrix. The number of MUs decomposed in each trial was more than 10. In random trials, the joint moved randomly between the initial position and the maximum joint angle position. Some MUs did not discharge in the movements during which the joint returned to the initial position before reaching the maximum joint angle position (see Fig. 5), probably because the activation threshold of these MUs was higher. When the EMG signals of flexor digitorum were decomposed, there will be some MUs that only represent the finger extension. It can be explored in future study whether the flexion/extension of MCP joint can be predicted with flexor digitorum only.

The surface EMG signals were acquired from the electrode grid covering the muscle. The electrode grid completely covered the muscle. The EMG signal of the target muscle acquired during the two-DoF simultaneous movements may be affected by the activation of adjacent muscles. After all, there were more than 40 muscles that may contribute to wrist and hand movements. In previous studies, the bipolar surface EMG electrodes were attached to the muscle for acquiring EMG signals [22]. Even if the optimal muscle position was found when the electrodes were attached and the distance between EMG sensors was large, the effect of adjacent muscles still existed. For example, it was observed

that the activation of the wrist flexor affected the EMG signal of the finger flexor [17]. This may be the reason why the r value of EMG-driven MM for MCP joint was only about 0.75 during two-DoF simultaneous movements. There was effect from adjacent muscles on the EMG signals with the bipolar surface EMG electrodes, and it is even more difficult for HD electrode grids to avoid such problems. The amplitude of the EMG signals acquired by the channel at the edge of the electrode grid was low and the effect of adjacent muscles also existed in the HD electrode grids. Therefore, it is not ideal to calculate the EMG envelope by directly averaging the 64 channels of the electrode grid. In this study, the optimal activation area of the muscle was found on the 8×8 electrode grid to simulate the bipolar EMG electrode acquisition and find the best position of the muscle for placing the electrode. The distance between the grid electrodes was close to that between the bipolar electrodes, so the 2×2 channels were selected as the optimal activation area. Channels in the optimal activation area of the muscle were selected and averaged to calculate the envelope. The estimation accuracy of the MM based on the calculated EMG envelope was similar to that of the previously reported EMG-driven MM [16], [22].

In recent years, a lot of machine learning methods have been proposed for simultaneous and proportional control of the hand and wrist. Nowak et al. proposed a three-DoF simultaneous and proportional estimator of hand and wrist movements based on ridge regression [42]. Sîmpetru et al. developed a new deep learning model that can reliably extract hand kinematics and dynamics from HD EMG data [43]. Sîmpetru et al. proposed the new deep learning model can predict hand movement in real-time with a constant prediction of 32 times per second [44]. These machine learning methods show good performance in predicting the continuous movements of the hand and wrist. Compared with machine learning methods, the decomposition of HD EMG may provide a more appropriate method from a physiological point of view, since it simulates how the central nervous system encodes muscle forces [45], [46]. In practice, there are many limitations in real-time decoding a significant number of MUs during the dynamic movement of the hand [47]. Real-time prediction of continuous movements is very important for practical applications. Therefore, the online decomposition method and the neural-driven MM should be investigated for real-time prediction of continuous movements in our future studies.

The proposed neural-driven MM provides accurate estimation of joint movements, which may be useful for medical rehabilitation and remote robot control. In addition, the proposed neural-driven MM can extract accurate neural information for the given task, even when HD EMG recordings are influenced by adjacent muscles. Therefore, the proposed neural-driven MM has the potential to extract accurate neural commands and improve the performance of HMIs established based on surface EMG signals. However, this study still has several limitations that need to be improved in the future. The proposed neural-driven MM was only validated on non-disabled subjects. Therefore, amputated subjects will be recruited to test the performance of the neural-driven MM in clinical applications. The current study was still an offline analysis, although online decomposition was employed. In future work, the performance of the proposed approach to predict continuous movements in real time and across days will be explored. Moreover, the study focused on the discharge of motor neurons at the population level, and did not refine the role of individual motor neuron. The proposed neural-driven MM cannot simulate the phenomenon that a motor neuron may innervate multiple muscles. In addition, only four muscles were included in the MM, and the simplification of the model may lead to joint movement prediction errors. Therefore, we will continue to improve our MM and prove the potential of this technique for medical rehabilitation in the future.

V. Conclusion

This study proposed a neural-driven MM to predict movements of the wrist and MCP joint. We used the FastICA algorithm to decompose the HD EMG signals, so as to obtain the MUs discharge and estimate the neural drive from the brain to the muscle. The neural drive was used as the input of MM to estimate the muscle activation. Ten non-disabled subjects (male) were recruited and tested. It was demonstrated that the proposed neural-driven MM can overcome several limitations of surface EMG signals and extract more accurate neural commands. The study quantitatively compared the performance of the neural-driven MM and conventional EMG-driven MM. The results indicated that the neural-driven MM outperforms the EMG-driven MM in prediction accuracy and robustness. The proposed neural-driven MM for HMI can identify neural commands more accurately and has great potential for medical rehabilitation and robot control.

Acknowledgment

The authors thank all the subjects for taking part in the experiments.

References

[1] A. Furui et al., "A myoelectric prosthetic hand with muscle synergy–based motion determination and impedance model–based biomimetic control," *Sci. Robot.*, vol. 4, no. 31, Jun. 2019, Art. no. eaaw6339.

[2] J. Chen, X. Zhang, Y. Cheng, and N. Xi, "Surface EMG based continuous estimation of human lower limb joint angles by using deep belief networks," *Biomed. Signal Process. Control*, vol. 40, pp. 335–342, Feb. 2018.

[3] T. Zhang, H. Sun, and Y. Zou, "An electromyography signals-based human–robot collaboration system for human motion intention recognition and realization," *Robot. Comput.-Integr. Manuf.*, vol. 77, Oct. 2022, Art. no. 102359.

[4] N. Jiang, K. B. Englehart, and P. A. Parker, "Extracting simultaneous and proportional neural control information for multiple-DOF prostheses from the surface electromyographic signal," *IEEE Trans. Biomed. Eng.*, vol. 56, no. 4, pp. 1070–1080, Apr. 2009.

[5] L. H. Smith, T. A. Kuiken, and L. J. Hargrove, "Evaluation of linear regression simultaneous myoelectric control using intramuscular EMG," *IEEE Trans. Biomed. Eng.*, vol. 63, no. 4, pp. 737–746, Apr. 2016.

[6] A. Ameri, E. N. Kamavuako, E. J. Scheme, K. B. Englehart, and P. A. Parker, "Support vector regression for improved real-time, simultaneous myoelectric control," *IEEE Trans. Neural Syst. Rehabil. Eng.*, vol. 22, no. 6, pp. 1198–1209, Nov. 2014.

[7] S. Muceli and D. Farina, "Simultaneous and proportional estimation of hand kinematics from EMG during mirrored movements at multiple degrees-of-freedom," *IEEE Trans. Neural Syst. Rehabil. Eng.*, vol. 20, no. 3, pp. 371–378, May 2012.

[8] Y. Yu, C. Chen, J. Zhao, X. Sheng, and X. Zhu, "Surface electromyography image-driven torque estimation of multi-DoF wrist movements," *IEEE Trans. Ind. Electron.*, vol. 69, no. 1, pp. 795–804, Jan. 2022.

[9] R. Roy, F. Xu, D. G. Kamper, and X. Hu, "A generic neural network model to estimate populational neural activity for robust neural decoding," *Comput. Biol. Med.*, vol. 144, May 2022, Art. no. 105359.

[10] W. Guo et al., "Multi-attention feature fusion network for accurate estimation of finger kinematics from surface electromyographic signals," *IEEE Trans. Hum.-Mach. Syst.*, vol. 53, no. 3, pp. 512–519, Jun. 2023.

[11] H. Su, W. Qi, Z. Li, Z. Chen, G. Ferrigno, and E. De Momi, "Deep neural network approach in EMG-based force estimation for human–robot interaction," *IEEE Trans. Artif. Intell.*, vol. 2, no. 5, pp. 404–412, Oct. 2021.

[12] G. Hajian and E. Morin, "Deep multi-scale fusion of convolutional neural networks for EMG-based movement estimation," *IEEE Trans. Neural Syst. Rehabil. Eng.*, vol. 30, pp. 486–495, 2022.

[13] C. Ma et al., "A bi-directional LSTM network for estimating continuous upper limb movement from surface electromyography," *IEEE Robot. Autom. Lett.*, vol. 6, no. 4, pp. 7217–7224, Oct. 2021.

[14] Y. Liu, S. Zhang, and M. Gowda, "Neuropose: 3D hand pose tracking using EMG wearables," in *Proc. Web Conf.* New York, NY, USA: Association for Computing Machinery, 2021, pp. 1471–1482, doi: 10.1145/3442381.3449890.

[15] C. Lin, X. Chen, W. Guo, N. Jiang, D. Farina, and J. Su, "A BERT based method for continuous estimation of cross-subject hand kinematics from surface electromyographic signals," *IEEE Trans. Neural Syst. Rehabil. Eng.*, vol. 31, pp. 87–96, 2023.

[16] L. Pan, D. L. Crouch, and H. Huang, "Comparing EMG-based human–machine interfaces for estimating continuous, coordinated movements," *IEEE Trans. Neural Syst. Rehabil. Eng.*, vol. 27, no. 10, pp. 2145–2154, Oct. 2019.

[17] J. Zhao, Y. Yu, X. Wang, S. Ma, X. Sheng, and X. Zhu, "A musculoskeletal model driven by muscle synergy-derived excitations for hand and wrist movements," *J. Neural Eng.*, vol. 19, no. 1, Feb. 2022, Art. no. 016027.

[18] B. J. Majors and J. S. Wayne, "Development and validation of a computational model for investigation of wrist biomechanics," *Ann. Biomed. Eng.*, vol. 39, no. 11, pp. 2807–2815, Nov. 2011.

[19] D. L. Crouch and H. Huang, "Musculoskeletal model predicts multi-joint wrist and hand movement from limited EMG control signals," in *Proc. 37th Annu. Int. Conf. IEEE Eng. Med. Biol. Soc. (EMBC)*, Aug. 2015, pp. 1132–1135.

[20] D. G. Lloyd and T. F. Besier, "An EMG-driven musculoskeletal model to estimate muscle forces and knee joint moments in vivo," *J. Biomechanics*, vol. 36, no. 6, pp. 765–776, Jun. 2003.

[21] T. S. Buchanan, D. G. Lloyd, K. Manal, and T. F. Besier, "Neuromusculoskeletal modeling: Estimation of muscle forces and joint moments and movements from measurements of neural command," *J. Appl. Biomechanics*, vol. 20, no. 4, pp. 367–395, Nov. 2004.

[22] D. L. Crouch and H. Huang, "Lumped-parameter electromyogram-driven musculoskeletal hand model: A potential platform for real-time prosthesis control," *J. Biomechanics*, vol. 49, no. 16, pp. 3901–3907, Dec. 2016.

[23] M. Sartori, G. Durandau, S. Došen, and D. Farina, "Robust simultaneous myoelectric control of multiple degrees of freedom in wrist-hand prostheses by real-time neuromusculoskeletal modeling," *J. Neural Eng.*, vol. 15, no. 6, Dec. 2018, Art. no. 066026.

[24] J. Li, R. Wang, and L. Pan, "An enhanced EMG-driven musculoskeletal model based on non-negative matrix factorization," *Biomed. Signal Process. Control*, vol. 79, Jan. 2023, Art. no. 104178.

[25] K. G. Keenan, D. Farina, K. S. Maluf, R. Merletti, and R. M. Enoka, "Influence of amplitude cancellation on the simulated surface electromyogram," *J. Appl. Physiol.*, vol. 98, no. 1, pp. 120–131, Jan. 2005.

[26] D. Farina et al., "Man/machine interface based on the discharge timings of spinal motor neurons after targeted muscle reinnervation," *Nature Biomed. Eng.*, vol. 1, no. 2, pp. 1–12, Feb. 2017.

[27] D. Farina, A. Holobar, R. Merletti, and R. M. Enoka, "Decoding the neural drive to muscles from the surface electromyogram," *Clin. Neurophysiol.*, vol. 121, no. 10, pp. 1616–1623, Oct. 2010. [Online]. Available: https://www.sciencedirect.com/science/article/pii/S1388245710003457

[28] C. Dai, Y. Zheng, and X. Hu, "Estimation of muscle force based on neural drive in a hemispheric stroke survivor," *Frontiers Neurol.*, vol. 9, p. 187, Mar. 2018. [Online]. Available: https://www.frontiersin.org/articles/10.3389/fneur.2018.00187

[29] Y. Zheng and X. Hu, "Concurrent estimation of finger flexion and extension forces using motoneuron discharge information," *IEEE Trans. Biomed. Eng.*, vol. 68, no. 5, pp. 1638–1645, May 2021.

[30] C. Dai and X. Hu, "Finger joint angle estimation based on motoneuron discharge activities," *IEEE J. Biomed. Health Informat.*, vol. 24, no. 3, pp. 760–767, Mar. 2020.

[31] C. K. Thompson et al., "Robust and accurate decoding of motoneuron behaviour and prediction of the resulting force output," *J. Physiol.*, vol. 596, no. 14, pp. 2643–2659, Jul. 2018.

[32] S. Yue, J. Li, and L. Pan, "A neural-driven musculoskeletal model for continuous estimation of hand and wrist movements," in *Proc. 12th Int. Conf. CYBER Technol. Automat., Control, Intell. Syst. (CYBER)*, 2022, pp. 856–860.

[33] A. Hyvärinen and E. Oja, "Independent component analysis: Algorithms and applications," *Neural Netw.*, vol. 13, nos. 4–5, pp. 411–430, Jun. 2000.

[34] C. Dai and X. Hu, "Independent component analysis based algorithms for high-density electromyogram decomposition: Experimental evaluation of upper extremity muscles," *Comput. Biol. Med.*, vol. 108, pp. 42–48, May 2019.

[35] F. Negro, S. Muceli, A. M. Castronovo, A. Holobar, and D. Farina, "Multi-channel intramuscular and surface EMG decomposition by convolutive blind source separation," *J. Neural Eng.*, vol. 13, no. 2, Apr. 2016, Art. no. 026027.

[36] C. Dai and X. Hu, "Independent component analysis based algorithms for high-density electromyogram decomposition: Systematic evaluation through simulation," *Comput. Biol. Med.*, vol. 109, pp. 171–181, Jun. 2019.

[37] A. Holobar and D. Zazula, "Multichannel blind source separation using convolution kernel compensation," *IEEE Trans. Signal Process.*, vol. 55, no. 9, pp. 4487–4496, Sep. 2007.

[38] Y. Ning, X. Zhu, S. Zhu, and Y. Zhang, "Surface EMG decomposition based on K-means clustering and convolution kernel compensation," *IEEE J. Biomed. Health Informat.*, vol. 19, no. 2, pp. 471–477, Mar. 2015.

[39] T. Kapelner, F. Negro, O. C. Aszmann, and D. Farina, "Decoding motor unit activity from forearm muscles: Perspectives for myoelectric control," *IEEE Trans. Neural Syst. Rehabil. Eng.*, vol. 26, no. 1, pp. 244–251, Jan. 2018.

[40] C. Chen, Y. Yu, X. Sheng, and X. Zhu, "Non-invasive analysis of motor unit activation during simultaneous and continuous wrist movements," *IEEE J. Biomed. Health Informat.*, vol. 26, no. 5, pp. 2106–2115, May 2022.

[41] N. Rubin, Y. Zheng, H. Huang, and X. Hu, "Finger force estimation using motor unit discharges across forearm postures," *IEEE Trans. Biomed. Eng.*, vol. 69, no. 9, pp. 2767–2775, Sep. 2022.

[42] M. Nowak, I. Vujaklija, A. Sturma, C. Castellini, and D. Farina, "Simultaneous and proportional real-time myocontrol of up to three degrees of freedom of the wrist and hand," *IEEE Trans. Biomed. Eng.*, vol. 70, no. 2, pp. 459–469, Feb. 2023.

[43] R. C. Sîmpetru et al., "Sensing the full dynamics of the human hand with a neural interface and deep learning," *bioRxiv*, p. 7, Dec. 2022.

[44] R. C. Sîmpetru, M. März, and A. Del Vecchio, "Proportional and simultaneous real-time control of the full human hand from high-density electromyography," *IEEE Trans. Neural Syst. Rehabil. Eng.*, vol. 31, pp. 3118–3131, 2023.

[45] D. S. de Oliveira et al., "You will grasp again: A direct spinal cord/computer interface with the spared motor neurons restores the dexterous control of the paralyzed hand after chronic spinal cord injury," *medRxiv*, 2022.

[46] A. Del Vecchio et al., "Spinal motoneurons of the human newborn are highly synchronized during leg movements," *Sci. Adv.*, vol. 6, no. 47, Nov. 2020, Art. no. eabc3916.

[47] A. Del Vecchio, A. Holobar, D. Falla, F. Felici, R. M. Enoka, and D. Farina, "Tutorial: Analysis of motor unit discharge characteristics from high-density surface EMG signals," *J. Electromyogr. Kinesiol.*, vol. 53, Aug. 2020, Art. no. 102426.